Astronomy & Astrophysics manuscript no. paper2a
March 14, 2008

The structure of the inner Oort cloud from the simulation of its formation for two giga-years

G. Leto[1], M. Jakubík[2], T. Paulech[3], L. Neslušan[2], and P. A. Dybczyński[4]

[1] Catania Astrophysical Observatory, Via Santa Sofia 78, I-95123 Catania, Italy
e-mail: gle@astrct.oact.inaf.it

[2] Astronomical Institute of the Slovak Academy of Sciences, 05960 Tatranská Lomnica, Slovakia
e-mail: mjakubik@ta3.sk; ne@ta3.sk

[3] Astronomical Institute of the Slovak Academy of Sciences, Dúbravská cesta 9, 84504 Bratislava, Slovakia
e-mail: astrotom@savba.sk

[4] Astronomical Observatory of the A. Mickiewicz University, Słoneczna 36, 60-286 Poznań, Poland
e-mail: dybol@amu.edu.pl

Received April 15, 2008; accepted ???? ??, ????

ABSTRACT

Aims. Considering the model of the initial disc of planetesimals consisting of 10 038 test particles, we simulated the formation of the distant comet reservoirs for the 2 -Gyr period. The result concerning an outer part of the Oort cloud was described in our previous paper. Here, using the resultant data from the simulation, we deal with the evolution of the population and structure at 2 Gyr of the complementary inner part of the Oort cloud.

Methods. The dynamical evolution of the massless test particles is followed via numerical integration of their orbits. We consider the perturbations by four giant planets on their current orbits and with their current masses, as well as the perturbations by the Galactic tide and passing stars.

Results. The efficiency of the formation of inner OC is found to be very low: only about 1.1% of all considered particles ended in this part of the comet cloud. The particles originated from the Uranus (35.5%), Neptune (35.4%), and Kuiper-belt (18.4%) regions of the initial proto-planetary disc, in particular. At 2 Gyr, the dynamics of the inner cloud is prevailingly governed by the dominant z-term of the Galactic tide. The number density of the bodies is proportional to the heliocentric distance, r, as $\propto r^{-3.53}$. The directional distributions of orbits is strongly inhomogeneous. There are, for example, large empty regions in the space angles around the Galactic Equator points with the galactic longitude 90^o and 270^o, or no bodies having the ecliptical latitude exceeding $\approx 150^o$. A strong inclination to the Ecliptic is apparent up to $\approx$ 900 AU (with a possible, but not exactly proved extension to $\approx$ 1 500 AU). Beyond $r \approx$ 6 000 AU, the bodies directly above the Sun, with respect to the Ecliptic, absent.

Key words. Comets: general – Oort cloud – Solar system: formation

1. Introduction

Dynamically *new* comets are those observed in the zone of visibility, which were not significantly perturbed by the planets during their former revolution around the Sun. This condition requires that their semi-major axis, a, must be larger than a certain critical limit, a_c. So, we can observe new comets with $a \geq a_c$ and deduce an existence of a corresponding comet reservoir. However, the absence of observation of new comets with $a < a_c$ does not necessarily imply a non-existence of the comets with $a < a_c$, detached from the planetary perturbations. Hills (1981) suggested the existence of the continual inward extension of the observationally-detected Oort cloud (OC, hereinafter), which is referred to as *inner OC*, at the present.

In a previous work (Dybczyński et al., 2008; this work is referred to as Paper I, hereinafter), we performed a simulation of the OC formation considering the massless test particles (TPs). The approximation of real planetesimals or cometary nuclei with the massless particles allows the using of the GRID-computing technique, with a number of mutually independent CPUs, that uses to be easier accessible than a super-computer. In our Paper-I simulation, we considered the model of the initial disc of planetesimals consisting of 10 038 TPs and studied their dynamics during 1 Gyr, when influenced the perturbations by the four giant planets (on their current orbits and with their current masses), Galactic tide, and nearly passing stars.

Send offprint requests to: L. Neslušan

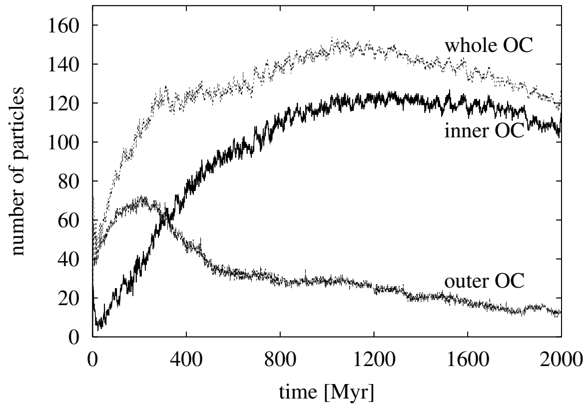

Fig. 1. The evolution of the population of the OC during the first two giga-years. The evolution of all, inner-OC, outer-OC, as well as whole-OC populations is demonstrated.

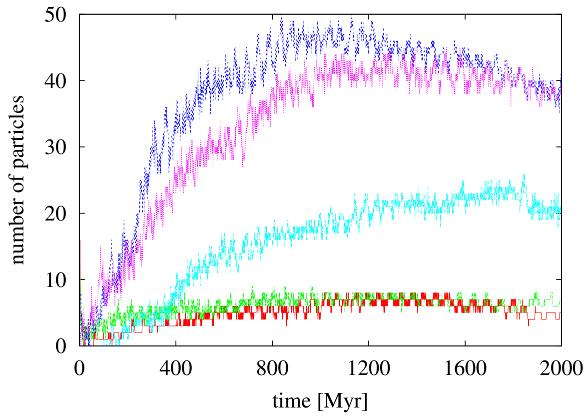

Fig. 2. The evolution of the delivery of comets to the inner OC, which initially originated in the Jupiter, Saturn, Uranus, Neptune, and Kuiper-belt regions. The contributions from these regions are illustrated by red, green, dark blue, violet, and light blue curves, respectively.

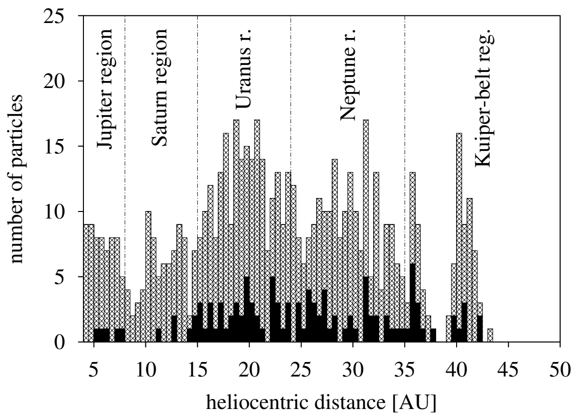

Fig. 3. The numbers of the TPs moved into the inner OC from the Jupiter, Saturn, Uranus, Neptune, and Kuiper-belt regions. The full bars illustrate the numbers of the TPs in 0.5 AU-wide intervals of the initial PPD, which reside in the inner OC at 2 Gyr. The empty bars do so for the TPs ever occuring, at least for a short period, in the inner OC. (The animation of the evolution of this dependence during the entire investigated period is available, in the *avi* format, on: http//www.ta3.sk/˜mjakubik/AstroDyn/INNER_OC_FORMATION/.)

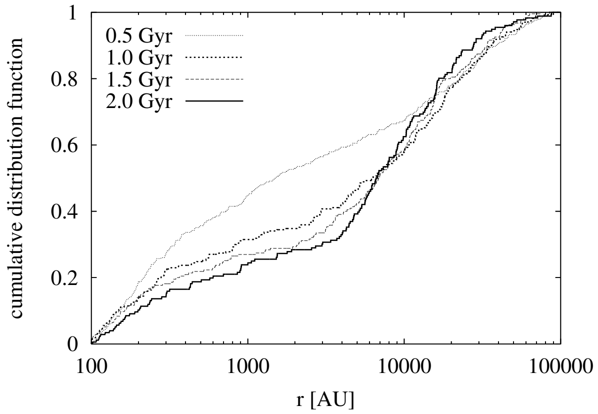

Fig. 4. The cumulative distribution function of the TPs after 500, 1000, 1500, and 2000 Myr. (The animation of the evolution of this dependence during the entire investigated period is available, in the *avi* format, on: http//www.ta3.sk/˜mjakubik/AstroDyn/INNER_OC_FORMATION/.)

(A more detailed description of the initial conditions and computational procedure used can be found in Paper I.) Based on this simulation, we described the formation and some structural characteristics of the outer part of the OC, in Paper I.

In the present work, we again use the resultant data from the former simulation, meanwhile extended for the period of 2 Gyr, and describe the formation process, further dynamical evolution, and some features of the structure of up-to-date hypothetical inner part of the OC.

2. The inner Oort cloud from our simulation

We classify a given TP as a member of the inner OC, if: its perihelion distance, q, is $q \geq 50$ AU and its semi-major axis, a, is $a \leq 25\,000$ AU.

2.1. Forming of the inner Oort cloud

The evolution of the inner-OC population is demonstrated in Fig. 1. The maximum population occurs at about 1 250 Myr. At the end of our simulation corresponding with the time of 2 Gyr, the population is represented with 110 TPs that implies 1.1% efficiency of the inner-OC formation. At this time, the population of the outer OC is represented only with about 13 TPs (0.13% formation efficiency). One can calculate that only 10% of the TPs, that reside in the OC, reside in its outer part at 2 *Gyr*.

Let us to compare our result with the analogous result obtained by Dones et al. (2005) (DLDW, hereinafter; see also Dones et al., 2004), we well as that obtained by Duncan et al. (1987; DQT87, hereinafter). To made a more consistent comparison, we re-define the inner and outer OC according DLDW: TPs are regarded as the members of the OC if their $q \geq 45$ AU, $a \geq 2\,000$ AU, and the border between the inner and outer clouds is at $a = 20\,000$ AU. For the re-defined

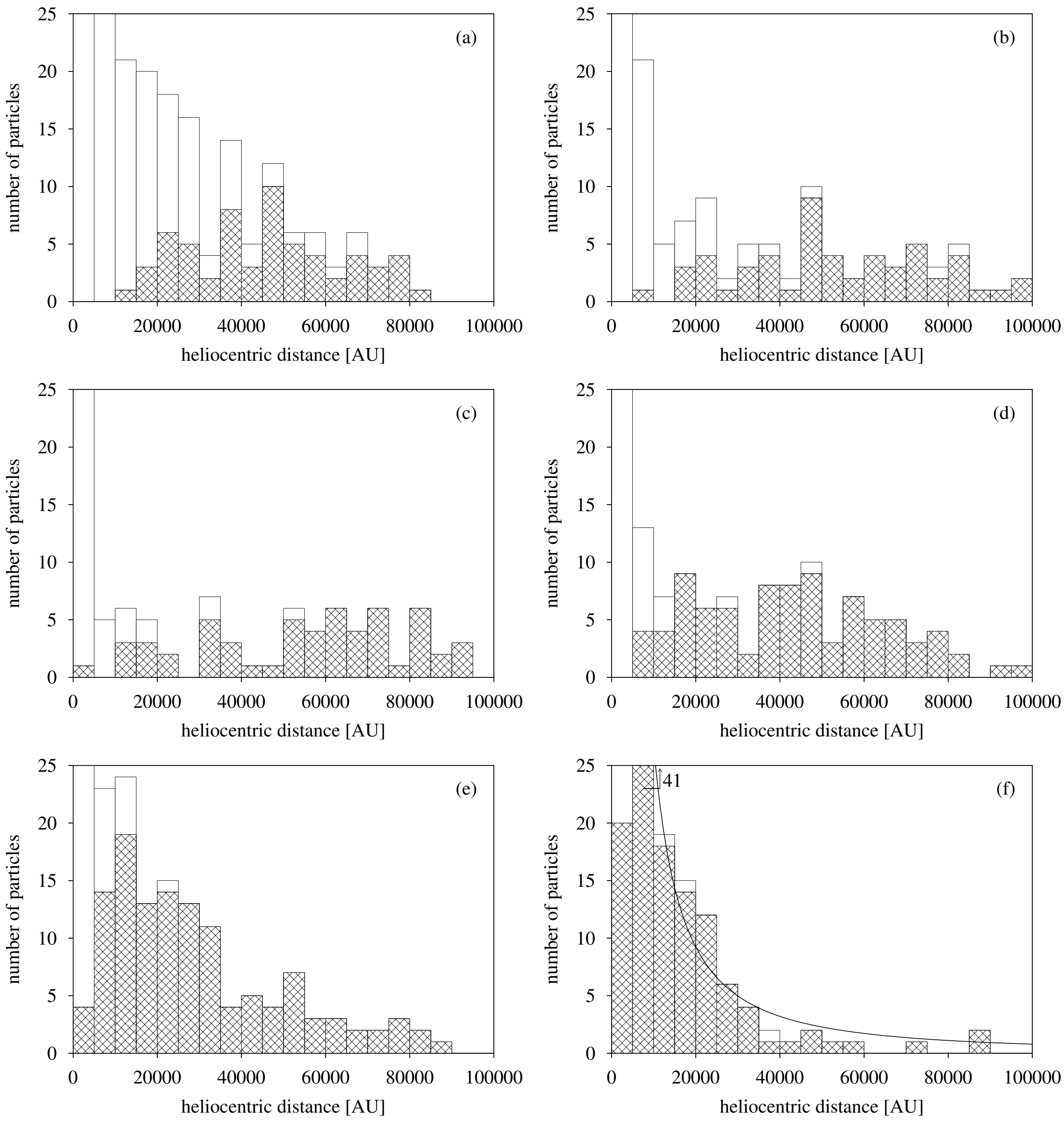

Fig. 5. The distribution of the heliocentric distance of OC comets (crosshatched bars) for the times of 2 (plot a), 8 (b), 31 (c), 125 (d), 500 (e), and 2 000 Myr (f). The corresponding distributions of all comets, still bound to the Sun, are also shown (empty bars). In the region $r < 10\,000$ AU, these distributions are outside of the chosen scale because of a better transparency of the first group of distributions (in plot f, the bar for $5\,000 < r < 10\,000$ AU is also out of the range; the actual value is given as numeral). If all comets in the given interval are in the OC, the crosshatched bar overlaps the empty bar, which is not visible in this interval, then. In plot f, our fit of the behaviour in the interval from 5 000 to 100 000 AU, by the power-law with index $s = -1.53$, is shown with the solid curve. (The animation of the evolution of this distribution during the entire investigated period is available, in the *avi* format, on: http//www.ta3.sk/˜mjakubik/AstroDyn/INNER_OC_FORMATION/.)

clouds, we can find 12% of all in-the-OC-situated TPs residing in its outer part. Even this value is much lower than the amount found by DLDW within so-called ',cold run'', which corresponds with the initial conditions assumed in our work, (about 48% of OC TPs in the outer OC), and also significantly lower than that found by DQT87 (about 20% of OC TPs in the outer OC). The fraction of TPs which came to the OC from the region of the proto-planetary disc (PPD) beyond 40 AU, not considered by DLDW, cannot account either for a small part of the discrepancy. These TPs enrich as the population of inner OC as that of outer OC. Summarily, the TPs coming from the KB region of the initial PPD even more increases the amount of the TPs in the inner OC (from 11% to the mentioned 12% in the case of our simulation). A large difference between our and DLDW's results concerning the inner-OC formation efficiency obviously occurs due to a shorter outer border of the OC considered by us, our more subtle model of stellar perturbations, as well as other reasons discussed in Paper I. The reason of the

Table 1. The end states, at 2 Gyr, of the TPs, which reside in various regions (the first column) of the PPD in the beginning of performed simulation. In the beginning, we consider the PPD consisting of 10 038 TPs. In the end of the simulation some of the TPs, from the given part of planetary region, still have their perihelion, q, in this region, i.e. $q < 50$ AU, or they are moved in the inner (IOC) or outer (OOC) Oort cloud, ejected into the interstellar space, or were destroyed at a collision with one of the considered massive bodies, mostly with the Sun. An asterisk indicates the average values from the period 991−2000 Myr, since the numbers still vary, in the given cases.

region	$q < 50$	in IOC*	in OOC*	ejected	collided
Jupiter	50	4.9	2.0	1389	187
Saturn	13	6.9	1.0	1802	260
Uranus	62	39.0	3.3	1596	367
Neptune	173	38.9	3.0	1443	390
KB	1734	20.2	3.3	439	122

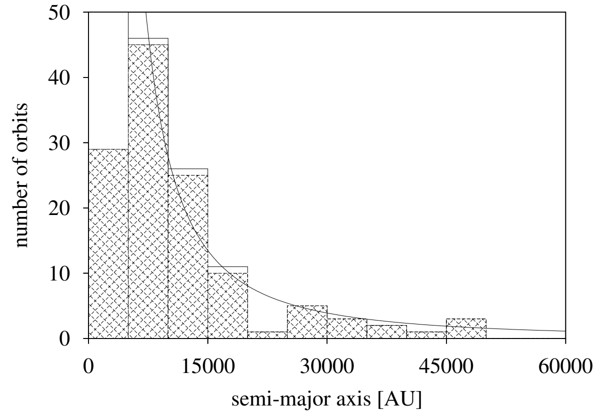

Fig. 6. The distribution of the orbital semi-major axis of TPs residing in the OC at 2 Gyr (crosshatched bars). The corresponding distribution of all comets, still bound to the Sun, is also shown (empty bars). In the interval from 5 000 to 50 000 AU, the behaviour is fitted by the power law with the index of slope $s_a = -1.736$ (solid curve). (The animation of the evolution of this distribution during the entire investigated period is available, in the *avi* format, on: http//www.ta3.sk/˜mjakubik/AstroDyn/INNER_OC_FORMATION/.)

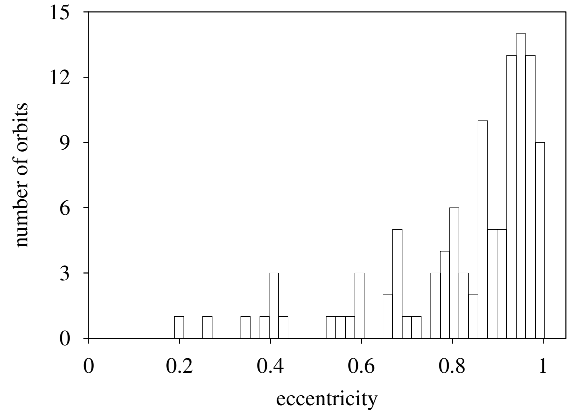

Fig. 7. The distribution of the orbital eccentricity of TPs residing in the inner OC at 2 Gyr. (The animation of the evolution of this distribution during the entire investigated period is available, in the *avi* format, on: http//www.ta3.sk/˜mjakubik/AstroDyn/INNER_OC_FORMATION/.)

difference in the time of the occurrence of inner-OC population maximum (1.2 Gyr in our vs. 1.8 Gyr in DLDW's simulation) is unknown.

All end states at 2 Gyr are summarized in Table 1 by the region of the initial PPD, in which the TPs originated. Concerning the contributions to the inner OC from the individual regions, these contributions are 4.5%, 6.3%, 35.5%, 35.4%, and 18.4% from the Jupiter, Saturn, Uranus, Neptune, and Edgeworth-Kuiper belt (KB, hereinafter), respectively. (The evolution of these contributions is also illustrated in Fig. 2). The listed ratios are similar to those relevant to the outer OC (Paper I), besides the expected lower amount of the TPs from Jupiter-Saturn region in a comparison with the Uranus-Neptune region. The distribution of the TPs situated in the inner OC at 2 Gyr by the region of their origin is also shown in Fig. 3. In contrast to the formation of the outer OC, a lot of TPs have come into the inner OC also from the initial heliocentric distance of 35 − 37 AU, which corresponds with the 3:2 mean-motion resonance with Neptune.

2.2. The radial structure of the inner OC

The cumulative distribution function and radial distribution of the TPs in several selected moments are illustrated in Fig. 4 and 5, respectively. At 2 Gyr, the number of TPs increases in the highest rate in the interval from ≈ 3 000 to ≈ 25 000 AU (Fig. 4). The behaviour of the radial distribution of TPs in the inner cloud is rather chaotic during an early stage of its formation (Fig. 5a-d). Only when the inner-OC population approaches its maximum, in ≈ 1 250 Myr (Fig. 5e mostly corresponds with this stage), and after the maximum (Fig. 5f), the inner cloud becomes more and more centrally concentrated. At 2 Gyr, the number density of the TPs residing in the OC in the interval $5\,000 < r < 100\,000$ AU can be fitted by the power law with the index of slope $s = -3.529^{+0.031}_{-0.024}$. (The corresponding behaviour of the heliocentric-distance distribution is illustrated with the solid curve in Fig. 5f). This value is almost consistent, within the determination uncertainty, with $s = -3.5$ found by DQT87 for 3 000 − −50 000 AU interval, but at 4.5 Gyr.

In Fig. 6, we show the distribution of semi-major axis of the TPs, which are situated in the OC at 2 Gyr. Also this distribution evidences the centrally concentrated OC. (A decrease in the inner-most interval of 0 − 5 000 AU is caused by the existence of the inner limit of the cloud due to its definition, not by a lack of TPs.) The behaviour in the 5 000 − 50 000 AU interval can be approximated by the power law with the index $s_a = -1.736^{+0.038}_{-0.028}$.

The information contained in the distribution of the semi-major axis is completed with the information being in the distribution of eccentricity of the inner-OC orbits at 2 Gyr, which can be seen in Fig. 7. At 2 Gyr, a prevailing part of TPs in the inner OC moves on highly eccentric orbits. One can notice that the eccentricities lower than about 0.2 are missing. The animation of the entire evolution of this distribution (*fig07.avi*) confirms an expected fact that the TPs come to the inner OC on

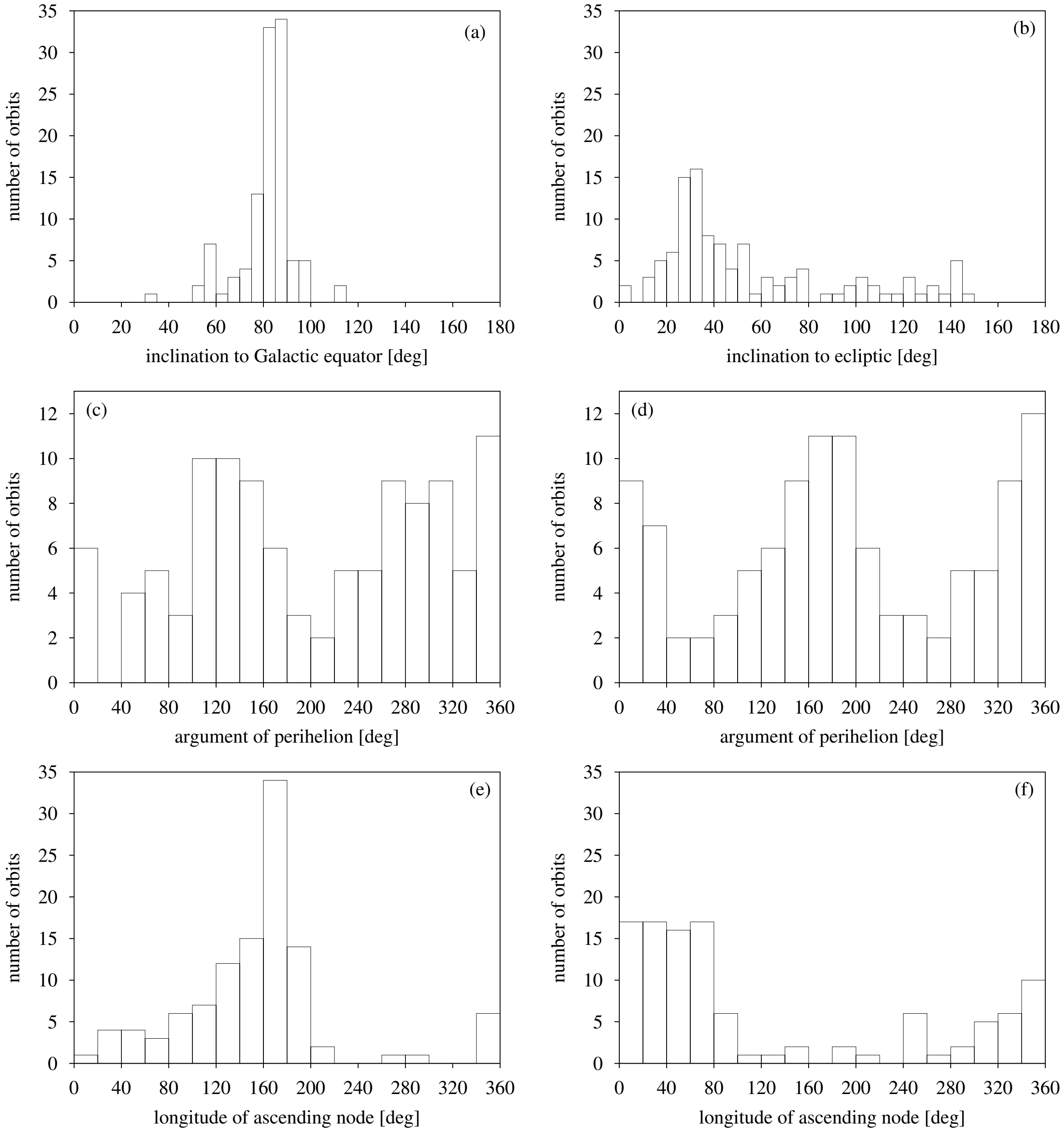

Fig. 8. The distributions of angular elements of TPs residing in the inner OC at 2 Gyr. The left-column plots demonstrate the distributions in the galactic coordinate frame, the right-column plots in the ecliptic coordinate frame. The pairs of plots (a)-(b), (c)-(d), and (e)-(f) demonstrate the distribution of the inclination (to the Galactic plane or to the Ecliptic), argument of perihelion, and longitude of ascending node, respectively. Notice the different vertical scale. (The animations of the evolution of these distributions during the entire investigated period are available, in the *avi* format, on: http//www.ta3.sk/˜mjakubik/AstroDyn/INNER_OC_FORMATION/.)

highly eccentric orbits, with $e \rightarrow 1$. Due to the libration of this element, which is coupled with the libration of the perihelion distance at an almost constant semi-major axis, some values of e lower than 0.98 begin to appear after 30 Myr. Then, the lower and lower values of the eccentricity start to appear. The down limit of ≈ 0.2 is reached after about 500 Myr. During the $500 - 2\,000$ Myr period, the values lower than 0.2 also occur, but only sporadically and for a short time. The typical distribution during this period is that shown in Fig. 7.

2.3. The orientation of the inner-OC orbits

In Fig. 8, there are demonstrated the distributions of angular orbital elements of the TPs, which stay in the inner OC at the end of the simulation (at 2 Gyr), in both galactic and ecliptical coordinate systems. Because of a relatively small numerousity of the TPs in the inner OC at the given time, the height of the bars in the plots slightly varies, when the plots are constructed for several, not very different times (e.g. 1 960, 1 980, 2 000 Myr). However, in all such mutually corresponding plots, we can see, in the galactic coordinates (left-column plots): (i) a

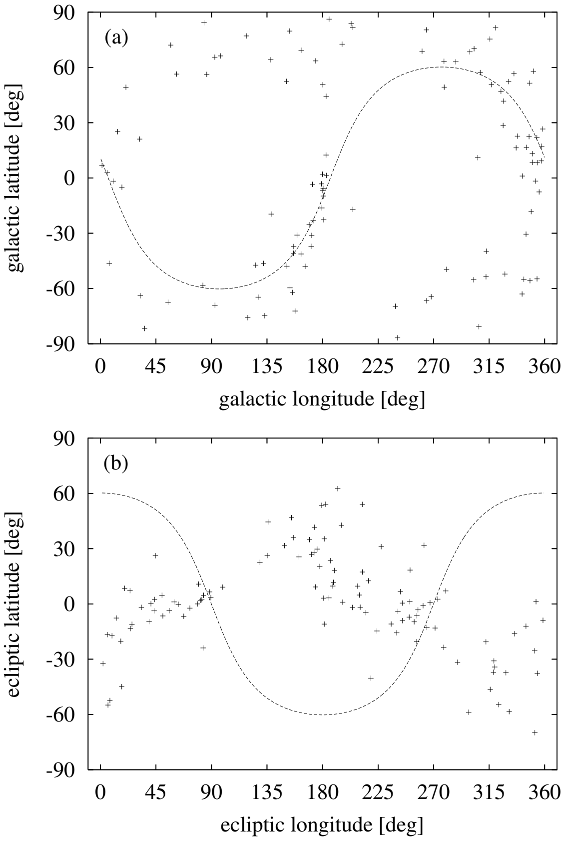

Fig. 9. The directional distribution of the aphelion points of TPs residing in the inner Oort cloud at 2 Gyr. Plot (a) demonstrates the distribution in the galactic coordinate frame, plot (b) does this in the ecliptic coordinate frame. The dashed curve shows the position of the Ecliptic in plot (a) and the position of the Galactic Equator in plot (b). (The animations of the evolution of these distributions during the entire investigated period are available, in the *avi* format, on: http//www.ta3.sk/˜mjakubik/AstroDyn/INNER_OC_FORMATION/.)

very hight peak at $\approx 80^o < i \approx 90^o$ and the zero-value or close-to-zero-value minima at $i < 55^o$ and $i > 100^o$ in plot (a) (see also animation *fig08a.avi*), (ii) the maxima at $90^o - 180^o$ and $260^o - 320^o$ intervals and minima at $0^o - 60^o$ and $180^o - 220^o$ intervals in plot (c), and (iii) the high maximum in $160^o - 180^o$ interval (a wider maximum in $140^o - 200^o$) and minimum in $220^o - 340^o$ interval in plot (e).

The corresponding features can be seen in the distributions constructed in the ecliptical coordinate system (right-column plots of Fig. 8). Seeing the plot showing the ecliptical distribution of the argument of perihelion (Fig. 8d) or the corresponding animation (*fig08c.avi*) from $\approx$ 300 Myr, the maxima in this distribution are related to the initial values, around 0^o and 180^o, at which the TP perihelia were detached from the planetary region by the Galactic tide. It seems that the argument of perihelion of a given TP typically retains, repeatedly, its initial value for a long period. Another information about the directional distribution of bodies in the inner OC can be deduced from Fig. 9 illustrating the directions of their aphelion points as well as from Fig. 10 giving the positions of some orbital elements in the dependence on the semi-major axis.

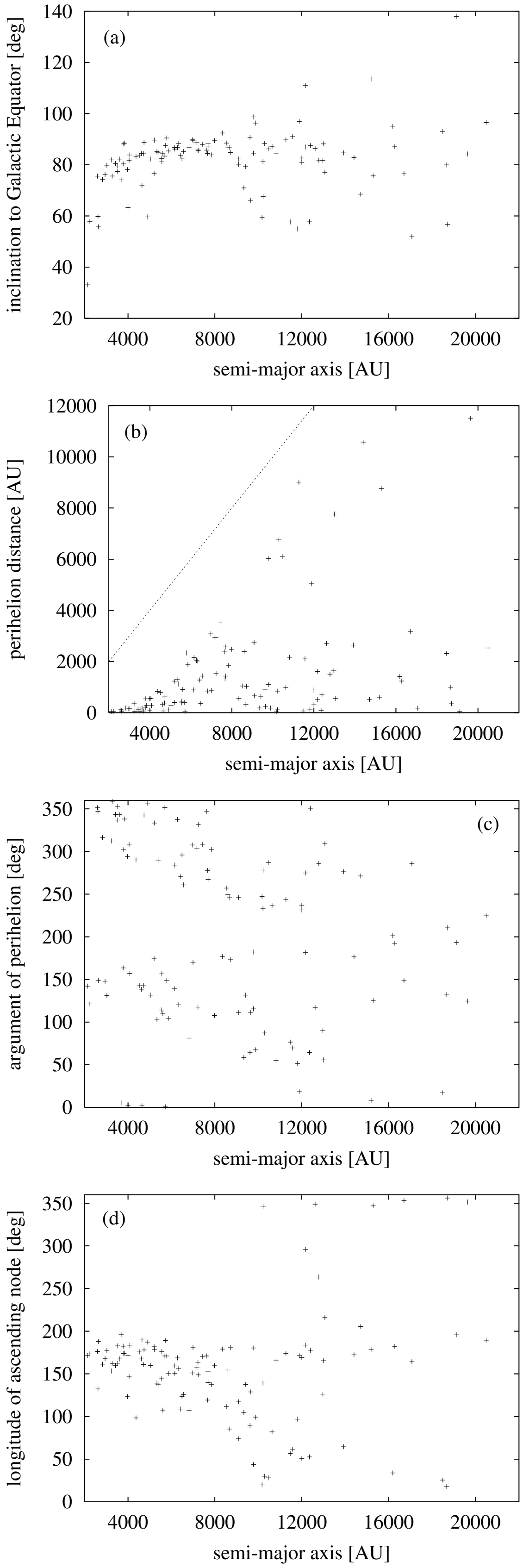

Fig. 10. The inclination to the Galactic Equator (a), perihelion distance (b), galactic argument of perihelion (c), and galactic longitude of ascending node of the TPs residing in the inner OC at 2 Gyr as the functions of their semi-major axis. The phase-space above the straight line in plot (b) is forbidden. (The animations of the evolution of these plots during the entire investigated period are available, in the *avi* format, on: http//www.ta3.sk/˜mjakubik/AstroDyn/INNER_OC_FORMATION/.)

All plots in Figs. 8 and 9 document the expected scenario of the formation of OC inner part. At the beginning (see also animation *fig09b.avi*), the comets are delivered to the inner OC on orbits inclined to the Ecliptic. The Galactic tide is mostly efficient when acting on the orbits with the aphelia in large distances (also large angular distances) from the Galactic-Equator plane (Galactic z-component of the aphelion point is large). So, these orbits are soon changed by the tide. The tide is less efficient in the case of comets approaching the inner OC on orbits inclined to the Galactic-equator plane. Here, the process of their change is relatively slow. Some orbits inclined to both Ecliptic and Galactic Equator can be seen surviving in a relatively low galactic-latitude region ($-45^o < b < +45^o$) in Fig. 9a. In the range of b between $\approx -45^o$ and $\approx +45^o$ far from the Ecliptic, there are almost no aphelia. It is well-known that the dominant z-term of the Galactic tide causes only the cyclic change of Galactic inclination, from a starting value to a value approaching 90^o in the same quadrant than the starting value. (A typical time behaviour of the galactic inclination of an OC comet can be seen in the paper by Neslušan & Jakubík, 2005, Fig. 4b.) Since the starting value must correspond with the position of the Ecliptic, which is inclined to the Galactic Equator by 60.2^o, we observe (Fig. 9b) almost no aphelia above the ecliptical latitude of $\approx +60^o$ and below $\approx -60^o$ (no starting position much exceeding these limits exists).

As mentioned in Paper I, the Galactic inclination of orbits with the very short perihelia in the minimum of the libration cycle of this element approaches the value of 90^o for a relatively long period due to the action of the dominant, z-term of Galactic tide. Therefore, the probability of the occurrence of an orbit with a very high Galactic inclination is high. This can explain the high peak in the interval of $80^o - 90^o$ in Fig. 8a (or in the interval $25^o - 35^o$ in Fig. 8b, with respect to the angle between the Ecliptic and Galactic-Equator planes).

The orbital momentum of the comets wandering to the OC obviously tends to be conserved, therefore the comets with the aphelia below the Galactic-Equator plane firstly cross the galactic-coordinate descending node, when going away from the Sun. The ascending node is crossed at their return to the perihelia. Oppositely, the comets with aphelia above the Galactic-Equator plane firstly cross the ascending node. So, we can observe two maxima in the argument-of-perihelion distribution (Fig. 9c), obviously corresponding with the below and above Galactic-Equator plane wandering comets, but only a single maximum in the ascending-node distribution (Fig. 8e). (We would observe two maxima in the latter, if the distribution of the outward-motion nodes was constructed, instead the distribution of ascending nodes, which can correspond with as outward as inward moving comets.) The galactic-coordinate maxima of the argument of perihelion, at $50^{0o} - 140^o$ and $270^o - 320^o$ intervals, obviously correspond with the galactic longitude of points of the Ecliptic being closest to the Galactic Poles, which is 276.3^o (at the North Pole) and 96.3^o (at the South Pole). A steady-state in the directional distribution demonstrated in Figs. 8c and 8e (or 8d and 8f) occurs at $\approx$ 300 Myr after the beginning (see animations *fig08c.avi*, *fig08d.avi*, *fig08e.avi*, and *fig08f.avi*).

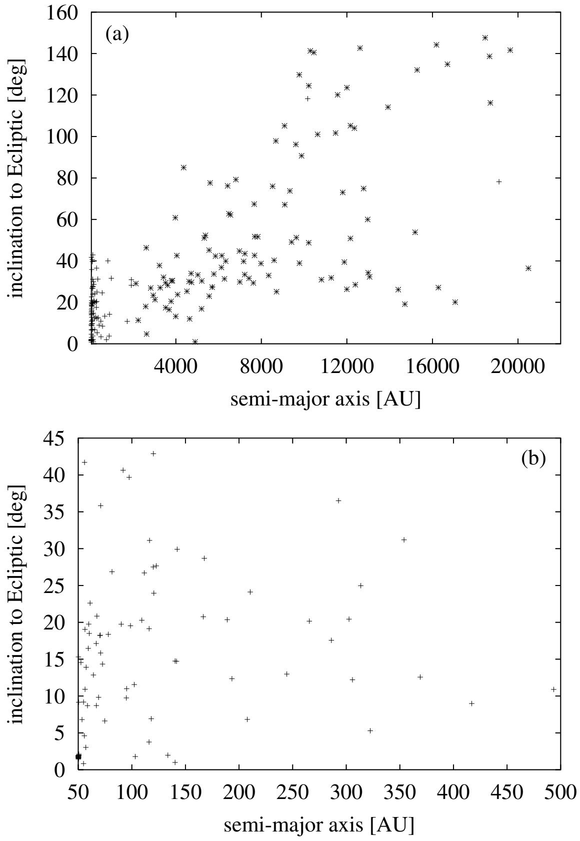

Fig. 11. The inclination to the Ecliptic vs. semi-major axis of the TPs on the orbits with semi-major axis in the interval $50 < a < 22\,000$ AU (a) and $50 < a < 500$ AU (b) at 2 Gyr. The TPs residing in this time in the inner OC are shown with asterisks, the other TPs with crosses. (The animations of the evolution of plot (a) as well as the more detailed view in plot (b) during the entire investigated period are available, in the *avi* format, on: http//www.ta3.sk/˜mjakubik/AstroDyn/INNER_OC_FORMATION/.)

The described distributions of the orbital elements of the TPs situated in the inner OC imply a large inhomogenity in the structure of this part of the OC. At 2 Gyr, this inhomogenity is not, however, caused by the origin of the TPs in a flat PPD. The dynamical memory is forgotten and the actual dynamics is governed by the dominant, z-term of the Galactic tide, in particular.

2.4. The flatteness of the inner OC

No empty regions exist between the populations of small bodies beyond the orbit of Neptune. The division into the scattered disc, extended scattered disc, and inner OC is established only for our methodological purpose. The trans-Neptunian disc, inclined to the Ecliptic, is expected to smoothly expand into a less and less flat region and gradually become a spherical comet cloud (inner OC). In this subsection, we attempt, on the basis of our simulation, to answer the question of how quickly the disc's inclination to the Ecliptic disappears and at what heliocentric distance the more or less spherically symmetric comet cloud occurs.

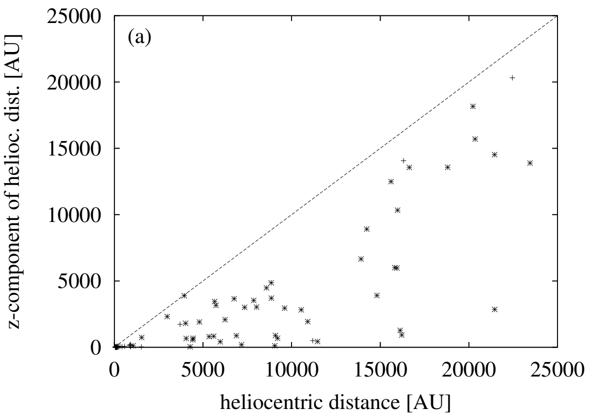

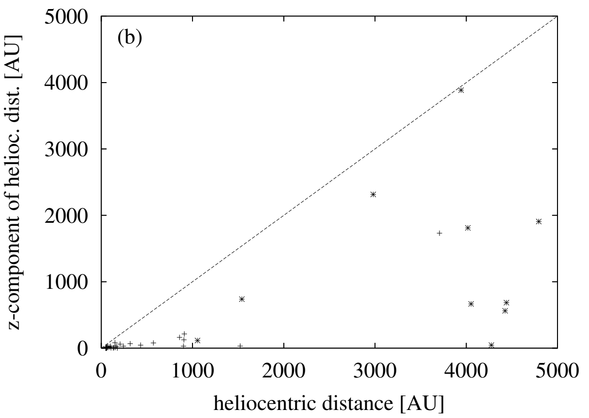

Fig. 12. The occurrence the TPs above the Ecliptic. Specifically, the ecliptical z-component of heliocentric distance vs. this distance of the TPs is shown, at 2 Gyr. In more detail, the TPs up to outer border of the inner OC are demonstrated. Plot (a) demonstrates the z vs. r distribution for $50 < r < 25\,000$ AU and plot (b) is a more detailed view of the $50 < r < 5\,000$ AU interval. The TPs residing at 2 Gyr in the inner OC are shown with asterisks, the other TPs with crosses. Since $z \leq r$, no TP can occur above the diagonal. (The animations of the evolution of plot (a) as well as the detailed view in plot (b) during the entire investigated period are available, in the *avi* format, on: http//www.ta3.sk/˜mjakubik/AstroDyn/INNER_OC_FORMATION/.)

The distribution of the TPs having their semi-major axes in the interval $50 < a < 25\,000$ AU in the $i - a$ phase space is illustrated in Fig. 11. (More exactly, the upper a in the plots is 22 000 AU, since there is no TP with a between 20 490 and 25 280 AU.) We can see that the larger and larger inclinations occur with the increasing semi-major axis. The PPD departures, step by step, from the Ecliptic. The inclinations larger than $\approx 45^o$ occur for $a \gtrapprox 4\,000$ AU and those larger than $\approx 90^o$ for $a \gtrapprox 8\,500$ AU.

An interesting phenomenon is an almost disappearance of the TPs with $i \lessapprox 20^o$ for $a \gtrapprox 5\,500$ AU. This phenomenon is likely caused by a special, at the moment unknown property of planetary perturbations, which enlarge the semi-major axis.

For $a \gtrapprox 10\,000$ AU, the inclination to the Ecliptic fills the entire interval from $\approx 20^o$ to $\approx 150^o$. However, it does not exceed $\approx 150^o$ even at the outer border of the inner OC. The reason of this phenomenon is clear from the animation *fig09b.avi* (see also Fig. 9b). The TPs firstly come to the OC on the orbits strongly inclined to the Ecliptic. In two intervals of the ecliptical longitude, these TPs rise highly above the Galactic-Equator plane, where are the subject of a stronger Galactic-tide perturbation than those TPs being close to the plane. From the distant-to-Ecliptic regions, the ecliptical inclinations of the TPs are changed to became large relatively to the Galactic Equator. Since the Galactic Equator is inclined to the Ecliptic about 60.2^o, the dominant z-term of the Galactic tide cannot increase any TP's aphelion to an ecliptical latitude larger than $\approx 60^o$ or lower than $\approx -60^o$. This circumstance is, then, reflected in the absence of ecliptic inclinations larger than $\approx 150^o$. Some exceptions can occur due to a weak action of the secondary terms of the Galactic tide or rare stellar perturbations.

The absence of orbits with the ecliptical $i \gtrapprox 150^o$ and $i \lessapprox 20^o$ (for $a \gtrapprox 5\,500$ AU) implies that the inner OC is not spherically symmetric in any part, and this fact does not allow to perform a more exact evaluation of the trans-Neptunian disc flatteness, with the more exactly determined characteristics.

The spatial flatteness of the trans-Neptunian disc can better be seen in the distribution of the ecliptical z-component of the TPs at the final time of the simulation (Fig. 12). Unfortunately, there are not very large numbers of the TPs in the critical intervals of heliocentric distance, r, in which the flatteness starts to disappear. Seeing a more central region $r < 5\,000$ AU (Fig. 12b), we can conclude that the disc is clearly inclined to the Ecliptic in the region of $r \lessapprox 900$ AU. Beyond this (but possible $r \approx 1\,500$ AU) distance, more TPs are situated at a larger distance from the Ecliptic. In the region between $3\,000 \lessapprox r \lessapprox 6\,000$ AU, our simulation does not exclude a disc that is, practically, spherically symmetric (but it does not either prove the symmetry due to a poor statistics). Beyond $r \approx 6\,000$ AU, the TPs situated directly above the Sun (with respect to the Ecliptic) absent. This absence is obviously linked to the absence of orbits with $i \gtrapprox 150^o$, which we discussed earlier.

3. Summary and discussion

Considering the model of the PPD consisting of 10 038 TPs and perturbations by four giant planets on their current orbits and with their current masses, as well as the perturbations by the Galactic tide and passing stars, we simulated the formation of the OC and the accompanying dynamical evolution of the Kuiper belt for the period of 2 Gyr. The properties of the inner OC we dealt with in this paper are following.

Its population quickly rises during the first mega-year due to the ejections of TPs from the Jupiter-Saturn region (Fig. 1). However, it immediately decreases and, from few mega-years after the beginning, it increases more or less linearly, with a high slope, untill about 500 Myr. Also after this time, the practically linear increase continues, but with a lower slope, till the maximum at about 1 250 Myr. Dividing the TPs in the inner OC by the region of their origin, we can conclude that the largest amounts originate from the Uranus and Neptune regions: 35.5% and 35.4%, respectively. The amount of the TPs originating in the KB region appears to be larger than each of the amounts from the Jupiter and Saturn regions from ≈ 500 Myr, and clearly exceeds these amounts at 2 Gyr. At this time, there are 4.5%, 6.3%, and 18.4% TPs originating in the Jupiter, Saturn, and KB regions, respectively, in the inner OC.

According our simulation and definitions of inner and outer OC, only about 10% of the TPs, that are in the OC at 2 Gyr, reside in the outer OC. The formation efficiency of the inner OC is 1, 1%. So, it is lower than the corresponding values obtained by previous authors (DQT87 obtained $\approx$ 20%; DLDW obtained 2.7% in their *cold* and 3.5% in their *hot run* for the inner OC).

At 2 Gyr, the number density of the TPs residing in the OC in the interval $5\,000 < r < 100\,000$ AU can be fitted by the power law with the index of slope $s = -3.529^{+0.031}_{-0.024}$. At the same time, the distribution of the semi-major axis in the $5\,000 - 50\,000$ AU interval can also be approximated by the power law with the index $s_a = -1.736^{+0.038}_{-0.028}$. The distribution of eccentricity of the inner-OC orbits implies that a prevailing part of TPs in the inner OC move on highly eccentric orbits. The eccentricities lower than about 0.2 are missing.

The orientation of the inner-OC orbits is strongly inhomogeneous. The inhomogenity can be seen in the distributions of the galactic-coordinate angular elements (Fig. 8). Specifically, there is a very hight peak at $\approx 80^o < i \approx 90^o$ and the zero-value or close-to-zero-value minima at $i < 55^o$ and $i > 100^o$ (see also animation *fig08a.avi*) in the distribution of inclination. Further, we can see the maxima at $90^o - 180^o$ and $260^o - 320^o$ intervals and minima at $0^o - 60^o$ and $180^o - 220^o$ intervals in the distribution of the argument of perihelion. And, the distribution of the longitude of ascending node has a high maximum in $160^o - 180^o$ interval and minimum in $220^o - 340^o$ interval. The corresponding features can also be seen in the distributions constructed in the ecliptical coordinate system. Moreover, it is possible to see that the inclination to the Ecliptic fills the entire interval from $\approx 20^o$ to $\approx 150^o$, for $a \gtrapprox 10\,000$ AU. However, it does not exceed the value of $\approx 150^o$ even at the outer border of the inner OC. The inhomogenity is also apparent from the plots of the directional distributions of aphelion points (Fig. 9). There are quite large empty regions around the Galactic-Equator points with the longitude of 90^o and 270^o. And, almost no aphelia can be seen in an ecliptical latitude higher than $+60^o$ or lower than -60^o. At 2 Gyr, the described inhomogenity is not, however, caused by the origin of the TPs in a flat PPD. The initial dynamical memory is forgotten and the actual dynamics is governed by the dominant, z-term of the Galactic tide, in particular.

The inner-most part of the inner OC is inclined to the Ecliptic as expected. With respect to the semi-major axis, the inclinations larger than $\approx 45^o$ occur for $a \gtrapprox 4\,000$ AU and those larger than $\approx 90^o$ for $a \gtrapprox 8\,500$ AU. The actual location of the TP position near the Ecliptic (low ecliptical z-coordinate) is apparent in the interval of heliocentric distance up to ≈ 900 AU. Beyond the distance of $\approx 6\,000$ AU, the TPs are also abundant at the large distances from the Ecliptic, except of the region directly above and below the Sun, with respect to the Ecliptic.

The electronic form of output data from the numerical integration of TP orbits, recorded every mega-year of the dynamical evolution, is available on: http//www.ta3.sk/˜mjakubik/AstroDyn/INNER_OC_FORMATION/ for the period from 1 to 2 Gyr. The animations of the evolution of distributions plotted in Figs. 3 to 12, for the entire period from 0 to 2 Gyr, are also available on this web site. The output data for the period from 0 to 1 Gyr are available on the web page http//www.ta3.sk/˜ne/OUTER_OC_FORMATION/ linked to Paper I.

Acknowledgements. G.L. thanks PI2S2 Project managed by the Consorzio COMETA, http://www.pi2s2.it and http://www.consorzio-cometa.it for the computational resources and technical support. M.J., T.P., and L.N. thank the project "Enabling Grids for E-sciencE II" (http://www.eu-egee.org/) for the provided computational capacity and support in a development of the computer code, which was necessary for a management of tasks on the GRID. They also acknowledge the partial support of this work by VEGA – the Slovak Grant Agency for Science (grant No. 7047).

References

Dones, L., Weissman, P.R., Levison, H.F., & Duncan, M.J. 2004, in: Comets II, eds. M. C. Festou, H. U. Keller, and H. A. Weaver (Arizona: Univ. Arizona Press), p. 153

Dones, L., Levison, H.F., Duncan, M.J., & Weissman, P.R. 2005, private communication

Duncan, M., Quinn, T., & Tremaine, S. 1987, AJ 94, 1330

Dybczyński, P.A., Leto, G., Jakubík, M., Paulech, T., & Neslušan, L. 2008, A&A, submitted (Paper I)

Hills, J.G. 1981, AJ 86, 1730

Neslušan, L. & Jakubík, M. 2005, A&A 437, 1093